Ion beam etching of lead-zirconate titanate thin films : correlation between etching parameters and electrical properties evomition

Caroline Soyer, Eric Cattan, Denis Remiens, Maryline Guilloux-Viry

HAL Id: hal-00149630

https://hal.science/hal-00149630

Submitted on 19 Aug 2022

Ion beam etching of lead–zirconate–titanate thin films: Correlation between etching parameters and electrical properties evolution

C. Soyer,[a] E. Cattan, and D. Rèmiens
Department of Materials for Integration in Microelectronics and Microsystems (MIMM), Université de Valenciennes, Z. I. du Champ de l'Abbessse, 59600 Maubeuge, France

M. Guilloux-Viry
Laboratory of Solid and Inorganic Molecular Chemistry (LCSIM), Institut de Chimie de Rennes, UMR 6511 CNRS–Université de Rennes 1, Campus de Beaulieu, 35042 Rennes, Cedex, France

Ion beam etching of sputtered $Pb(Zr_x,Ti_{1-x})O_3$ (PZT) with x equal to 0.54 thin films grown on $Pt/Ti/SiO_2/Si$ substrates has been performed using pure Ar gas. The etch rate dependence on the process parameters (current density, acceleration voltage, gas pressure) has been investigated. The PZT etch rate can reach 600 Å/min with acceleration voltage of 1000 V and current density of 1 mA/cm^2. Selectivity ratios between PZT and masks of various natures (photoresist, Pt, Ti) have been evaluated to determine a pertinent material for etching mask. According to our etching conditions, titanium seems to be the best candidate. We evaluated the PZT surface damage by contact mode atomic force microscopy. It appears that the roughness increases after ion bombardment, and that the grain boundary zone is preferentially etched. For some etching parameters, we also observed electrical damage. Carrying out $C(V)$ and hysteresis loops $P(E)$ measurements before and after etching have provided evidence of degradation. We noted a large decrease in permittivity after the etching process irrespective of the current density and acceleration voltage. Ferroelectric damage was illustrated by a large increase in the average coercive field. For each of the electrical properties under study, the same behavior has been observed after etching: the increase of damage was obtained as a function of the current density and acceleration voltage. The evolution of electrical properties when the PZT layer is protected by a metallic mask has also been studied. We observed very slight variations in the electrical properties.

I. INTRODUCTION

Great interest in ferroelectric thin films has developed for application in memory devices [dynamic random access memory (DRAM) and ferroelectric random access memory (FeRAM)] and in microelectromechanical systems (MEMS). $Pb(Zr_x,Ti_{1-x})O_3$ (PZT) thin films are one of the most used materials because of their interesting electrical properties, as well as being both ferroelectric and piezoelectric. Patterning of PZT films has become an essential element of device fabrication. Several techniques have been developed for etching: wet chemical etching,[1] ion beam etching (IBE),[2] reactive ion etching (RIE),[3–5] electron cyclotron resonance (ECR) etching,[6] and inductively coupled plasma (ICP) etching.[7]

RIE is widely used because it provides, under some etching conditions, a high etch rate, high degree of anisotropy, and selectivity. Various gas mixtures for etching have been investigated: $Cl_2/C_2F_6/Ar$,[7] Cl_2/Ar,[6] $CF_4/CCl_4/Ar$,[8] and Cl_2/BCl_3.[9] The influence of the etching parameters on the evolution of electrical damage has already been studied in the case of chemically assisted bombardment. It seems that neither the effect of physical damage nor the presence of residual chemical species on the film surface has not yet been studied separately. However, it is currently assumed that par-

ticle bombardment is primarily responsible for the etching whatever the process.[10,11] Moreover, for MEMS applications, the possibility of etching a global structure, such as a bottom electrode/ferroelectric film/top electrode, that includes several materials without having to change the etching gas' composition is a very interesting aspect of pure ion etching.

In this work, we study pure-Ar ion beam etching on ferroelectric PZT thin films, and Ti, Pt, and photoresist as etching masks. The influence of the etching parameters is investigated in terms of the etch rate and selectivity. The surface roughness and evolution of the electrical properties of maskless PZT are also evaluated. The feasibility of using a metallic mask has already been demonstrated, particularly for RIE. A Pt mask was used by Pan *et al.*[5] and for platinum films etching, Chiang *et al.*[12] used a TiN mask. In this article, by using the selectivity ratio of PZT/Ti, we study the etching of Pt/PZT/Pt capacitors masked with a Ti layer. Ti sputtering follows deposition of a Pt-top electrode. The evolution of the PZT electrical properties is systematically evaluated as a function of the discharge parameters.

II. EXPERIMENTAL PROCEDURE

Several samples with PZT, Pt and Ti films, were grown separately for etch rate and selectivity evaluation. Pt and Ti layers of 500 nm were deposited on SiO_2/Si substrates by dc sputtering. $Pb(Zr_{0.54},Ti_{0.46})O_3$ thin films were deposited on

---

[a])Electronic mail: caroline.soyer@univ-valenciennes.fr

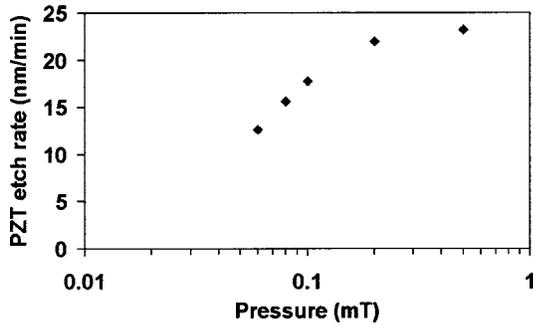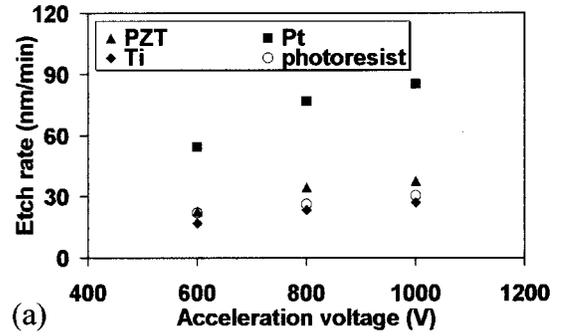FIG. 1. Etch rate of PZT as a function of the pressure (acceleration voltage=800 V, current density=0.6 mA/cm^2).

FIG. 2. Evolution of the etch rate (a) and selectivity (b) as a function of the acceleration voltage (current density=0.7 mA/cm^2).

Pt/Ti/SiO$_2$/Si substrates by rf magnetron sputtering and they had a thicknesses ranging from 0.9 to 1.2 μm. The sputtering conditions are given elsewhere.[13] The PZT films were annealed at 625 °C for 30 min to form PZT perovskite phase. All the samples were (110) preferentially oriented, with no pyrochlore phase being evident.

Ion beam etching of PZT, Pt, and Ti was investigated by the Veeco Microetch 3 in. This system was equipped with a Kaufman type source. It incorporates a filament electron-emitting cathode, an electromagnet mounted on the outside of the ion source chamber. The ion extraction and acceleration systems consist of a three-grid assembly. Argon ions were extracted by the acceleration potential (typically between 0.6 and 1 kV). The current density can be adjusted to the value desired by adjusting the magnetic field, pressure, arc power, and cathode emission. A filament allows the positive charge of the ion beam (neutralizing filament) to be neutralized. The sample holder is water cooled. The sample temperature is stabilized after an etching of more than 5 min. So, we have taken care to exceed this delay for each process performed.

Several films were coated with conventional photoresist (Microposit® S1813 from Shipley) that was patterned by exposure in a mask aligner. The etch thickness was determined by a Tencor surface profilometer. The surface microstructure of unetched and etched PZT was characterized by atomic force microscopy (AFM). Images in contact mode AFM were obtained using a Park Scientific Instruments Autoprobe CP. Some samples were observed by scanning electron microscopy (SEM) using a field effect JEOL JSM 6301 F microscope. A low working voltage of 9 kV allowed observation of the samples without prior metallization.

Pt top electrodes were sputtered through a shadow mask on etched PZT to determine the evolution of the electrical properties. They were then compared to the unetched samples to evaluate the extent of the IBE effect. Capacity, tan δ, and $C(V)$ measurements were performed using an impedance analyzer (HP4192A), at frequency of 10 kHz and voltage of V_{ac}=100 mV. The ferroelectric loops $P(E)$ were measured using a standard Radiant RT6000 system. The charge option was used, so the top electrode was always connected to the drive terminal of the test equipment, while the bottom electrode was connected to the return terminal.
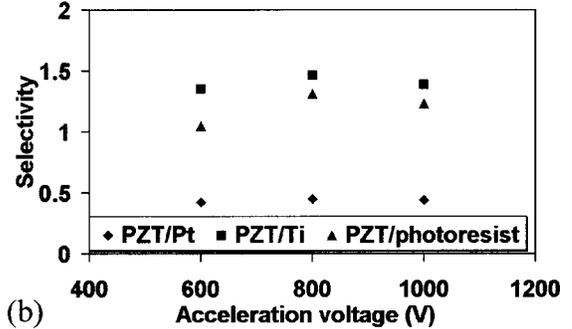
Measurements were made before and after top electrode annealing contact at 500 °C.

III. RESULTS AND DISCUSSION

A. Etch rate and selectivity ratio

Ion milling with an inert gas was performed in order to evaluate the characteristics of pure physical bombardment under an argon beam. Figure 1 shows the variation of the PZT etch rate with the pressure. In this example, the acceleration voltage was fixed to 600 V and the current density was 0.6 mA/cm^2. The etch rate increases rapidly with an increase in pressure (in the range of 0.05–0.1 mTorr), and seems to become constant between 0.2 and 0.5 mTorr. With our experimental system, it was difficult to reach stable pressure better than 1 mTorr. For higher pressure, we should observe a decrease in the etch rate. The same behavior was observed whatever the process parameters. The values of the PZT etch rate ranged from 12 to 23 nm/min. Since our intent was to work at a high etch rate, the pressure was fixed at 0.2 mTorr.

The etch rate of PZT and the feasibility of using photoresist, Pt, and Ti as etch masks were first examined as functions of the etching conditions including the ion density and acceleration voltage. We maintained a constant etching time. Figures 2(a) and 2(b) illustrate, respectively, the evolution of the etch rate and the selectivity ratio as a function of the acceleration voltage (the current density is fixed at 0.7 mA/cm^2). We observe an increase in the etch rate with an increase in acceleration voltage, whatever the etched material. On the other hand, we consider that the selectivity, defined as the ratio between the PZT etch rate and the Pt, Ti, or photoresist etch rate, remains relatively constant. Figures
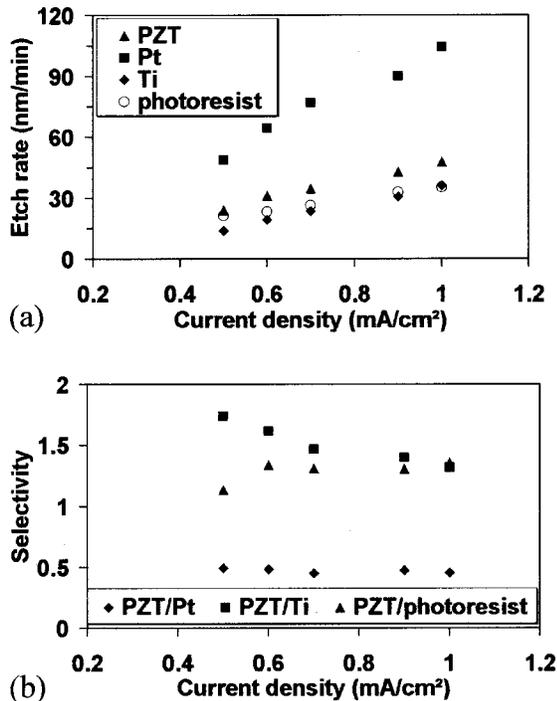
FIG. 3. Evolution of the etch rate (a) and selectivity (b) as a function of the current density (acceleration voltage=800 V).

TABLE I. Influence of etching on the PZT roughness.

	Global roughness (Å)	Local roughness (Å)
Unetched PZT	60	48
Etched PZT (600 V, 0.7 mA/cm²)	229	148
Etched PZT (1000 V, 0.7 mA/cm²)	413	258
Etched PZT (800 V, 0.5 mA/cm²)	192	105
Etched PZT (800 V, 1 mA/cm²)	392	229

3(a) and 3(b) show the same evolution as a function of the current density. The acceleration voltage is fixed at 800 V, this allows coverage on a large current density scale. The etch rate of each material increases linearly with an increase in current density. Such behavior has currently been observed for ion beam etching as well as for RIE.[7,14] For a current density increase from 0.5 to 1 mA/cm², the PZT and Pt etch rates are twice as large. The Ti etch rate increases more rapidly (it is multiplied by 2.6). The best selectivity is obtained for the PZT/Ti ratio; the value of the ratio can reach 1.8 for low current density. In order to achieve an appreciable selectivity ratio, it is quite evident that it is desirable to have as low a current density as possible for a given acceleration voltage. For example, we can reach selectivity of PZT to Ti equal to 2.2 for acceleration voltage of 600 V and density of 0.4 mA/cm². By another way, a maximum PZT etch rate of 60 nm/min was obtained at 1000 V and 1 mA/cm²; however, the best selectivity is not achieved with these parameters. So, to find a good compromise between the etch rate and selectivity, it seems that the best etching conditions are a current density as low as possible and a high acceleration voltage.

The etch rate and the selectivity are important parameters with which to characterize the etching process, but it is well known that ion beam etching can induce degradation of the materials. So, we now focus on evaluation of surface and electrical damage due to Ar ion bombardment.

B. Influence of etching on the surface morphology

The influence of etching parameters in terms of surface morphology was examined using AFM in contact mode and obtained 30×30 μm² scanning micrographs. It appears to be necessary to distinguish two types of roughness. On one hand, the ''global'' roughness is measured on the total scanning surface. However, this root mean square (rms) roughness takes into account the grain boundary zone that appears to be very deep after etching. On the other hand, ''local'' roughness can be extracted by excluding the grain boundaries. This local roughness is more representative of the real roughness of the grain surface. The rms measured are summarized in Table I. Table I presents the global and local rms of unetched and etched PZT; in all cases, rms is defined as the root mean square. The results are given first as a function of the acceleration voltage, with a current density of 0.7 mA/cm², and after as a function of the current density with acceleration voltage fixed at 800 V. The results are in agreement with those obtained by scanning 50×50 μ and 15×15 μm² surfaces. Table I underscores the difference between local (48 Å) and global (60 Å) roughness that already exists for unetched PZT.

For comparison, the surface of the unetched PZT thin films is shown in Fig. 4(a). Figures 4(b) and 4(c) show the surface morphology of PZT etched with various acceleration voltages (600 and 1000 V). The surface morphology follows the same behavior as that varying the current density.

We measure an increase of roughness after etching for global as well as for local roughness. After etching, the difference between the local and global roughness is due to the grain boundary zone that appears to become increasingly wide and deep with an increase of the acceleration voltage or current density. The ratio of global roughness/local roughness is between 1.5 and 1.8, without any particular trend. This demonstrates that modification of the process parameters does not particularly favor etching at the grain boundaries more than on the grain surface. The values of the ratio also indicate that the grain boundaries are preferentially etched. This behavior is probably the result of two phenomena combined. Compositional variation between the grain and the boundary, in particular excess lead at the grain boundaries, could justify the deeper etching in these zones. The lead oxide etch rate is higher than the titanium or zirconium oxide etch rate. Lateral etching that induces boundary widening could add to the etching process. Excess physical atom bombardment can occur at the grain boundaries. It is well known in etch technology that the reflection of ions from the sidewalls generates a so-called trenching phenomenon. Unetched PZT already shows sharp grain boundaries. In this case, ion rebounding likely occurs at these grain boundary ''walls,'' and that could explain enhancement of the etch rate at this location.

The high local rms values obtained after etching mean that the grain surface is also damaged. Before etching, the grains are very flat and the surface microstructure is very
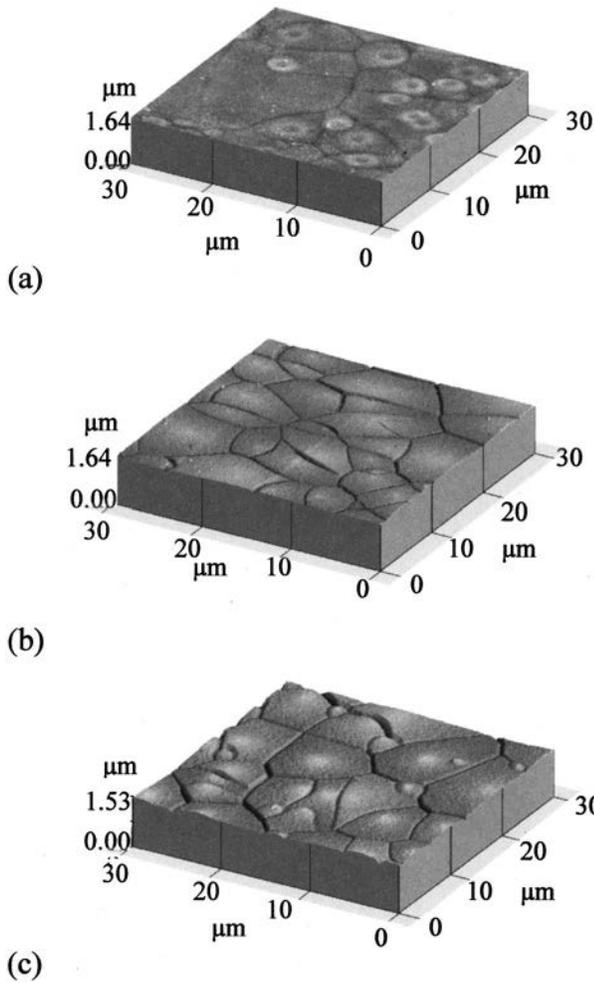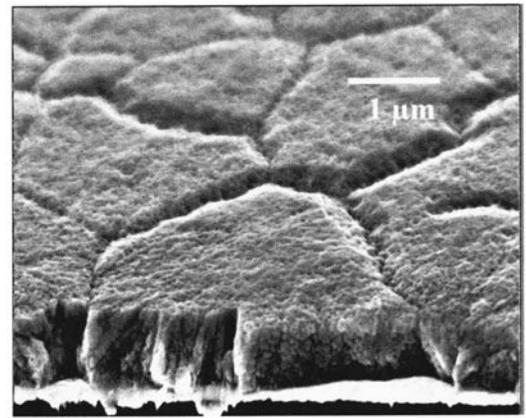
3

FIG. 4. 30×30 μm^2 AFM micrographs of (a) unetched PZT, (b) PZT etched at 600 V and 0.7 mA/cm^2, and (c) PZT etched at 1000 V and 0.7 mA/cm^2.

FIG. 5. SEM cross-sectional view of (a) etched PZT (800 V, 0.5 mA/cm^2) and (b) PZT etch profile.

dense. After ion bombardment, the surface seems to be more or less porous, whereas the grains become slightly rounded particularly when the current density and the acceleration voltage are at high values. Figure 5(a) presents a cross-sectional view of etched PZT and Fig. 5(b) allows one to compare unetched/etched PZT surfaces and to observe the etching profiles. The unetched surface was protected by a photoresist layer during the etching process. These SEM micrographs show that grain boundary widening occurs only at low depth, and they confirm the increase in surface roughness after etching. Moreover, from Fig. 5(b), we can see that a high degree of anisotropy is reached under our etching conditions.
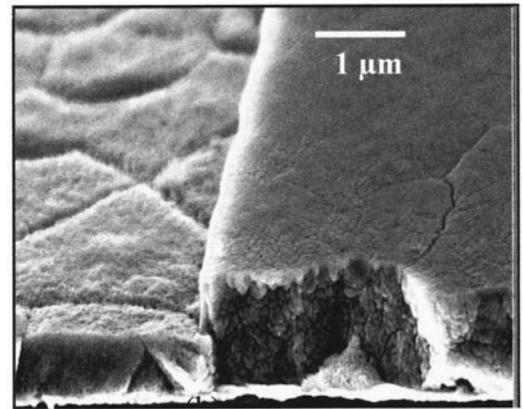
In conclusion, we suggest that there are two types of degradation during ion bombardment. Not only are the grain microstructure surfaces disturbed, the grain boundaries are also preferentially etched. The PZT roughness increases when the current density and the acceleration voltage increase.

C. Electrical damage

Study of the electrical properties as a function of the etching parameters was divided into two parts.

We first considered electrical damage in the case of maskless PZT etching. After etching under various conditions (by varying the acceleration voltage and the current density), the same final thickness of approximately 0.5 μm was obtained for all the samples. We systematically compared the electrical properties of unetched and etched PZT films. New Pt top electrodes were deposited on etched PZT followed by contact annealing (ca).

The second part of the study consists of investigation of the electrical damage induced in the case of PZT etching with a protective mask. We have chosen to use the Ti mask layer because of the superior selectivity ratio measured in comparison with the other masks tested. A Pt/PZT/Pt structure were prepared, and electrically characterized. Ti dots were deposited by lithography and liftoff onto the Pt top electrode. After having completely etched the Ti layer, new electrical measurements were performed on the Pt electrode. We have taken care to characterize exactly the same electrodes before and after etching.

It is essential to note that we systematically performed contact annealing when a top electrode was sputtered on an unetched PZT thin film. In the absence of top electrode annealing, a systematical shift of the hysteresis loop was observed toward the negative electric field direction, also re-
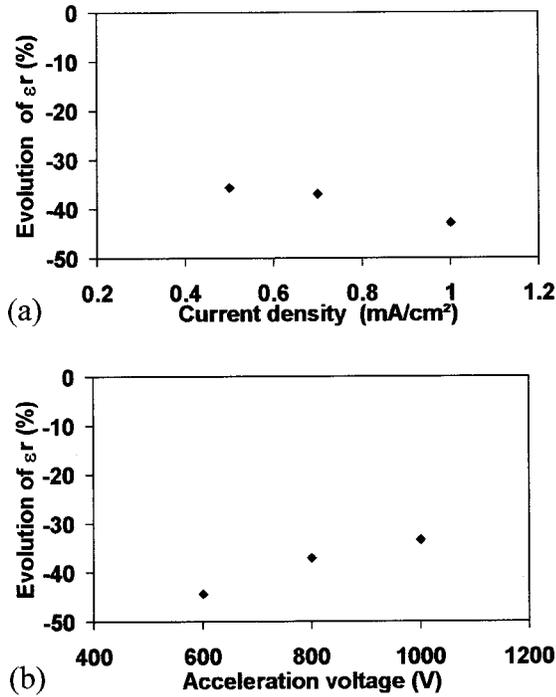
FIG. 7. Schematic cross-sectional view of our etched PZT thin film.

in thickness which was shown in different previous papers.[16,17] For our films especially, we have shown that ε_r remained constant above 0.6 μm and decreased under this thickness. For film thickness ranging from 0.6 to 0.5 μm, we have observed a 10% loss in permittivity; this cannot justify the value of ε_r obtained after etching.

As observed previously, the PZT surface is degraded by ion bombardment. The reduction in ε_r might be explained by the presence of roughness, amorphized material, and charged or neutral defects on the film surface and at the grain boundaries. This damage layer present on surface can be considered to have lower permittivity than ferroelectric PZT and this can induce a smaller dielectric constant for the global structure. If the surface damage layer has a capacitance of C_{surf}, then the apparent capacitance of the film C_{tot} is related to C_{surf} as follows:

$$1/C_{tot} = 1/C_{film} + 1/C_{surf},$$

where C_{film} is the capacitance of the undisturbed PZT film thickness.

The surface damage layer can be divided into two layers, as seen in Fig. 7. The first layer, denoted 1, would consist most especially of a amorphized material, lattice disorder, and atom implantation. The second layer, denoted 2, includes the same defects to which we have to add the roughness. We believe that these two layers are not ferroelectric. When we have previously suggested that the PZT film thickness was 0.5 μm after etching, we have not taken these layers into account. They reduce the "real" ferroelectric PZT thickness, and thus induce a more important decrease in ε_r.

When we consider the evolution of the permittivity as a function of the acceleration voltage, it appears that ε_r is reduced more at low acceleration voltage, whereas the surface roughness increases with an increase in acceleration voltage. So, the roughness (layer 2 in Fig. 7) is not the predominant factor in the permittivity decrease and layer 1 appears to be mainly responsible for the evolution observed. We suggest several hypotheses that could occur at low acceleration voltage:

(1) the layer 1 permittivity is lower;
(2) the layer 1 thickness is higher;
(3) layer 1 induces more important pinning at the interface with layer 0: the higher the layer 1 thickness, the lower the layer 0 one, and in this case, the influence of the defects present in layer 1 is stronger and stronger. The 180° domain wall motion is considered to be partly responsible for the permittivity. It was estimated that about 25%–50% of the dielectric response at room temperature

FIG. 6. ε_r evolution as a function of the (a) current density (acceleration voltage = 800 V) and (b) acceleration voltage (current density = 0.7 mA/cm²).

ported by Okamura et al.[15] without any particular decrease in the Pm (maximal polarization) or Pr (remanent polarization) observed. The shift indicates the development of an internal electric field (E_i) in the direction of the top electrode to the bottom electrode. After contact annealing at 500 °C for 30 min in air, the shift in the hysteresis loop partially disappears and the E_i was reduced from approximately −9 to −3 kV/cm. During the Pt sputtering process, charge is accumulated at the interface between the top electrode and the PZT film, which builds up the internal field. Charge trapping can be released from trap sites during the electrode annealing process. Moreover, the permittivity increases slightly (typically 9%–15%) after contact annealing. For greater clarity in the presentations of our results, we have given them in the percentage of decrease (−) or percentage of increase (+) compared to in the unetched PZT.

1. Etching of a maskless PZT

The results given here consist of a comparison of the permittivity measured before and after etching, and after Pt top contact annealing in both cases.

As shown in Figs. 6(a) and 6(b), the permittivity ε_r decreases significantly after the etching process. ε_r is damaged more at high current density and at low acceleration voltage. For example, the value of the permittivity can be reduced from 830 to 520 with current density and acceleration voltage fixed at 0.7 mA/cm² and 800 V, respectively.

For the same current density, particles of high energy produce fewer defects. This result shows clearly that rather than atom energy bombarding the film surface it is the increase in atom density that instigates a stronger lowering of the permittivity. This decrease is in part due to the decrease
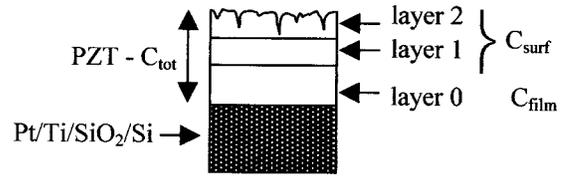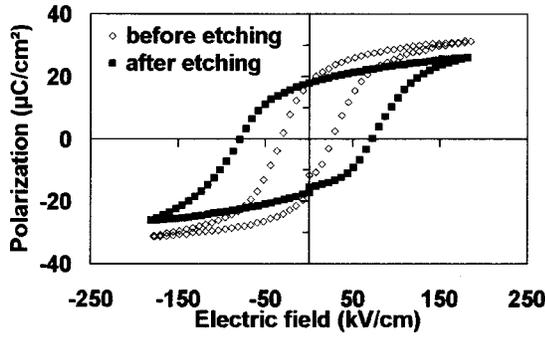
FIG. 8. $P(E)$ hysteresis loop of as-deposited PZT and etched PZT (800 V, 0.7 mA/cm^2) after contact annealing.
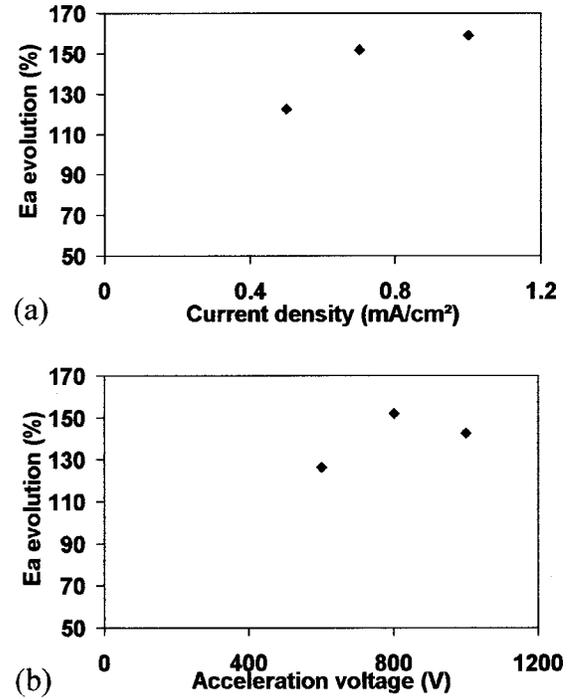

FIG. 9. Evolution of the average coercive field as a function of the (a) current density (acceleration voltage = 800 V) and (b) acceleration voltage (current density = 0.7 mA/cm^2).

is due to an extrinsic source.[18] Therefore, the decrease in permittivity could be linked to domain wall pinning.

We think it's unlikely that a low acceleration voltage can induce lower permittivity or a more important pinning phenomenon than a high acceleration voltage. On the other hand, for high acceleration voltage, we suggest that the etching is more efficient in comparison with the rate of creation of the damage layer (layer 1). As a result, the layer 1 thickness is higher at low acceleration voltage, and it appears to be the main factor in justifying the evolution of the permittivity.

With regard now to the evolution of the permittivity as a function of the current density, we have noted that the decrease in ε_r with an increase in current density coincides with an increase in roughness. However, we have explained previously that the layer 2 roughness cannot be the predominant parameter. We again think that layer 1 is responsible for the results observed, and we formulate the same assumptions as the previous ones. We consider that an increase in current density induces growth of the defect density. These many defects can involve a decrease in the layer 1 permittivity or, a larger domain wall pinning in the rest of the PZT film (layer 0). On the other hand, it seems unlikely that an increase in current density can modify the layer 1 thickness.

The evolution of maximal and remanent polarization, Pm and Pr, follows the same behavior as that already observed for the permittivity, and the hypothesis could have been the same. However, the hysteresis loops measured after etching show a decrease in maximum polarization (of between 15% and 25%) while the average remanent polarization is modified little, except for a weak acceleration voltage and strong current density. The very weak decrease in remanent polarization suggests that an important pinning phenomenon may occur that prevents the domain from switching back. One result from these observations is that the hysteresis loop is squarer.

The remarkable part of the hysteresis loop after etching film and top electrode annealing is the large increase in the average coercive field E_a. E_a is defined as $E_a = (|E_c^+| + |E_c^-|)/2$. We can see, for example, in Fig. 8 the $P(E)$ curve obtained for PZT etched at 800 V and 0.7 mA/cm^2. Similar

loop widening, of various magnitude, was observed for all etched samples. The magnitude of E_a was measured as a function of discharge parameters such as the current density and voltage acceleration and the results are shown in Fig. 9. The etching process has decreased the film thickness and it is currently assumed that the average coercive field increases with a decrease in thickness. So, as observed for the permittivity, the E_a increase can in part be attributed to the decrease in thickness;[19] for our films, an increase of approximately 35% is observed when the film thickness is reduced from 1 to 0.5 μm. Moreover, the "real" ferroelectric PZT thickness is reduced by the presence of the degraded layers (as explained earlier with regard to the dielectric properties) at the film top surface; this has also a strong effect on the increase of the coercive field. But we think that it is necessary to introduce other phenomena to explain the coercive field variations since E_a, under some etching conditions, can double.

When the acceleration voltage and current density increase, the average coercive field follows an evolution similar to that of local and global roughness. We suggest that the damage zone at the film surface is directly responsible for the E_a increase. The internal field remains very small and we conclude that few charged defects are present.

When we compare the hysteresis loop of etched thin films, before and after top electrode contact annealing, we observe many differences (Fig. 10). Before contact annealing, an internal electric field was observed for etched as well as for unetched PZT. However, this internal field achieves higher values (ranging from −17 to −23 kV/cm) for etched
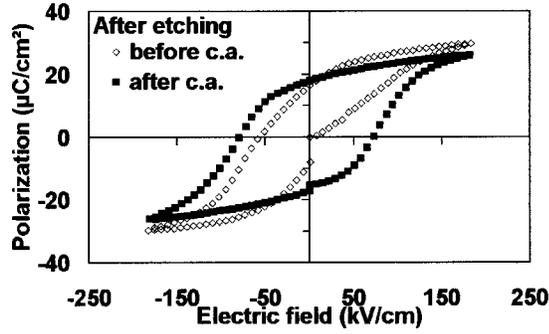
6

FIG. 10. $P(E)$ hysteresis loop of etched PZT (800 V, 0.7 mA/cm^2), before and after contact annealing.

FIG. 11. $P(E)$ hysteresis loop of as-deposited PZT and of etched PZT protected with a Ti mask layer (800 V, 1 mA/cm^2), after 500 °C annealing.

PZT, whatever the etching parameters. The appearance of E_i is assumed to be due to charge defects at the PZT/Pt interface, or to the presence of a mechanical stress gradient.[20] The presence of charge defects can be attributed to the deposit of the top electrode as previously explained, and only the etching process can justify the difference observed in the internal field measurement. However, we cannot explain the E_i increase, especially since the particles bombarding the surface are atoms. We suggest that the internal field makes switching the domain easier when we apply an electrical field in the same direction. That could justify the weak value of E_c^+ in comparison with that of $|E_c^-|$. However, $|E_c^-|$ is higher than the result measured for the unetched film. After contact annealing, the internal field is partially suppressed and switching is difficult in both directions; then, we have approximately the same values for E_c^+ and $|E_c^-|$. $|E_c^-|$ increased after contact annealing while generally, for an unetched PZT film, $|E_c^-|$ remains unchanged before and after ca. This difference between $|E_c^-|$ before and after ca indicates that annealing is responsible for part of the increase in E_a; during annealing, it's possible that defects induced by atom bombardment move or change, and that could justify an increase of the pinning phenomenon. By preventing domain wall motion, a higher electrical field is necessary to allow domain switching. A 500 °C annealing is basically not able to modify layers 1 and 2 (Fig. 7). On the other hand, a 500 °C annealing causes crossover of the Curie temperature and, therefore, we think that modification of the domain distribution and domain walls motion activates defects, and induces pinning.

2. Etching of PZT protected by a Ti mask layer

The use of a metallic etching mask in titanium sputtered on the platinum top electrode is a simple technological solution. We have observed that the selectivity of PZT to Ti is 2.2 and is about 4.7 for Pt to Ti. AFM observations have shown a weak increase in the platinum electrode surface roughness after titanium has been completely etched. Studies are underway to evaluate the sidewall angle around 65° from our first evaluations. Possible rotation and tilting of the substrate holder might improve these values. This study is now in progress.

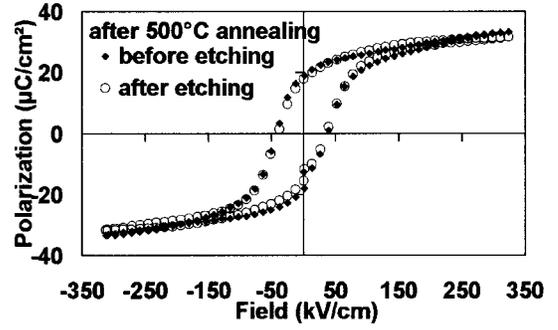A systematic ferroelectric properties study taking into consideration the acceleration voltage and the current density was performed. The thickness of the deposited titanium mask is calculated in order to have a similar etching time for each sample whatever the beam conditions. The final etched PZT thickness of around 400 nm is almost identical for each sample. Electrical measurements, in that case, were carried out on the same electrode before depositing titanium (on platinum top annealed electrode) and after complete etching of the titanium. The results obtained show that the electrical behavior of the material changes very little whatever the etching conditions. So, we suppose that the PZT films protected by a Ti mask do not degrade during ion beam etching. The observed variations in the electrical properties could be attributed to a incomplete etching of the titanium layer on the Pt top electrode, or to degradation of the Pt top electrodes after etching (roughness, the presence of charge etc.). The permittivity and maximal and remanent polarization as well as the coercive field decrease 15% to the maximum. The internal field increases significantly. We did not note any particular evolution with the acceleration and current density conditions. The results obtained are of the same order as those observed when we characterized an unetched sample after Pt top electrode deposition and before contact annealing. So, the property evolution induced by Ti layer etching can be compared to that observed when we sputter a top electrode. Annealing the etched structure at 500 °C allowed recovery of a hysteresis loop that is very similar to the one recorded before etching. The final dielectric and ferroelectric properties are only about 5% lower than initially; this is included in the error measurements. Figure 11 presents the hysteresis loops obtained before and after etching, in both cases after annealing.

IV. CONCLUSION

In this work, we have presented results of Ar-ion beam etching of PZT thin films. The PZT etch rate increases with an increase in the current density, acceleration voltage, and pressure. Several materials were tested as etching masks, and it appears that the best selectivity ratio was obtained using a titanium metallic mask. A good compromise between the etch rate and selectivity can be achieved by working at high acceleration voltages and low current densities.

We have shown that maskless PZT etching generates a large amount of damage in terms of surface morphology and electrical properties. Globally, the PZT roughness is much greater after etching, whatever the etching parameters and, more especially, it increases more and more with an increase in the current density and acceleration voltage. We have also observed widening of the grain boundaries; the grain boundaries are preferentially etched, probably due to the presence of an excess of lead at the joint grains.

When we compared the electrical results after contact annealing, before and after etching, we obtained the following evolution: the permittivity is largely reduced, the maximum polarization decreases whereas the remanent polarization is only modified a little, the average coercive field increases, and the internal field remains practically unchanged. We have proposed various hypotheses to explain these phenomena. The decrease in thickness is of course responsible for part of the evolution observed. We also considered that the global PZT film can be divided into several layers: one corresponding to an amorphized zone with implantation and lattice disorder, a second that includes the same defects as well as surface roughness, and finally a PZT layer without damage, except for possible domain wall pinning induced by the presence of the other layers. The comparison of ferroelectric properties after etching, before and after contact annealing, showed that annealing is in part responsible for the pinning phenomenon, probably because of defect activity.

Study is underway to examine the influence of a postetching annealing treatment to improve the electrical properties and repair surface damage.

Finally, we have also controlled the etching effects on PZT protected with a titanium mask. The PZT electrical properties are globally preserved, whatever the etching process, after 500 °C annealing.

[1] S. Mancha, Ferroelectrics **135**, 131 (1992).

[2] T. Kawagughi, H. Adachi, K. Setsune, O. Yamazaki, and K. Wasa, Appl. Opt. **23**, 2187 (1984).

[3] K. Saito, J. H. Choi, T. Fukuda, and M. Ohue, Jpn. J. Appl. Phys., Part 2 **31**, L1260 (1992).

[4] D. P. Vijay, S. B. Desu, and W. Pan, J. Electrochem. Soc. **140**, 2635 (1993).

[5] W. Pan, S. B. Desu, I. K. Yoo, and D. P. Vijay, J. Mater. Res. **9**, 2976 (1994).

[6] S. Yokoyama, Y. Ito, K. Ishihara, K. Hamada, T. Ohnishi, J. Kudo, and K. Sakiyama, Jpn. J. Appl. Phys., Part 1 **34**, 767 (1995).

[7] C. W. Chung and C. J. Kim, Jpn. J. Appl. Phys., Part 1 **36**, 2747 (1997).

[8] J. Baborowski, P. Muralt, N. Ledermann, E. Colla, A. Seifert, S. Gentil, and N. Setter, Integr. Ferroelectr. **31**, 261 (2001).

[9] N. Ikegami, T. Matsui, and J. Kanamori, Jpn. J. Appl. Phys., Part 1 **35**, 2505 (1996).

[10] J. J. Van Glabbeek, G. A. C. M. Spierings, M. J. E. Ulenaers, G. J. M. Mans, and P. K. Larsen, Mater. Res. Soc. Symp. Proc. **310**, 127 (1993).

[11] G. Suchaneck, R. Tews, and G. Gerlach, Surf. Coat. Technol. **116–119**, 456 (1999).

[12] M.-C. Chiang, F.-M. Pan, H.-C. Cheng, J.-S. Liu, and S.-H. Chan, J. Vac. Sci. Technol. A **18**, 181 (2000).

[13] G. Velu, D. Rèmiens, and B. Thierry, J. Eur. Ceram. Soc. **17**, 1749 (1997).

[14] T. Ting-Ao, C. Zheng, L. Ning, Z. Si-Xun, Ferroelectrics **232**, 47 (1999).

[15] S. Okamura, S. Miyata, Y. Mizutani, T. Nishida, and T. Shiosaki, Jpn. J. Appl. Phys., Part 1 **38**, 5364 (1999).

[16] R. Kurchania and S. J. Milne, J. Mater. Res. **14**, 1852 (1999).

[17] H. Fujisawa, S. Nakashima, M. Shimizu, and H. Niu, Proceedings of the Eleventh IEEE International Symposium Applications of Ferroelectrics, Montreux, Switzerland, 1998, p. 77.

[18] F. Xu, S. Trolier-McKinstry, W. Pen, B. Xu, Z.-L. Xie, and K. J. Hemker, J. Appl. Phys. **89**, 1336 (2000).

[19] R. Seveno, P. Limousin, D. Averty, J.-L. Chartier, R. Le Bihan, and H. W. Gundel, J. Eur. Ceram. Soc. **20**, 2025 (2000).

[20] E. G. Lee, J. S. Park, J. K. Lee, and J. G. Lee, Thin Solid Films **310**, 327 (1997).